Available online at www.sciencedirect.com
ScienceDirect
European Journal of Pharmaceutics and Biopharmaceutics 70 (2008) 389–401
European Journal of Pharmaceutics and Biopharmaceutics
www.elsevier.com/locate/ejpb

Research paper

Effect of the spraying conditions and nozzle design on the shape and size distribution of particles obtained with supercritical fluid drying

Andréanne Bouchard [a,*], Nataša Jovanović [b], Anne H. de Boer [c], Ángel Martín [d], Wim Jiskoot [b,e], Daan J.A. Crommelin [b], Gerard W. Hofland [a], Geert-Jan Witkamp [a]

[a] Process Equipment, Delft University of Technology, Delft, The Netherlands
[b] Department of Pharmaceutics, Utrecht University, Utrecht, The Netherlands
[c] Department of Pharmaceutical Technology and Biopharmacy, University of Groningen, Groningen, The Netherlands
[d] Departamento de Ingeniería Química y Tecnología del Medio Ambiente, Universidad de Valladolid, Valladolid, Spain
[e] Division of Drug Delivery Technology, Leiden University, Leiden, The Netherlands

Received 20 August 2007; accepted in revised form 31 March 2008
Available online 11 April 2008

Abstract

In the perspective of production of dry therapeutic protein formulations, spray drying of lysozyme (as a model protein) into supercritical carbon dioxide was studied. The effects of the nozzle (i.e., co-current coaxial converging and converging–diverging, and T-mixer impinging) and process conditions (i.e., flow rates, pressure) on the drying of the lysozyme prepared in aqueous solution dried with supercritical carbon dioxide enriched with ethanol were investigated. The particle size distribution, width of particle size distribution and morphology were used to determine the effect of the various parameters assessed. Particles with a median size of ~1.5, ~5 or ~25 μm were produced depending of the nozzle selected. A basic comparative study of the nozzle was done by computational fluid dynamics, but the differences in particle size could not be depicted by these computations. The proportional increase of the flow rates (up to fivefold) caused a decrease in particle size (7- to 12-fold), and doubling the pressure caused a moderate decrease of the size (5–20%). The individual effect of the supercritical carbon dioxide, ethanol and solution streams was explained with a mass transfer model. Changing the ratio between flow rates slightly affected the particle size in various ways because of the swelling and shrinking stages of the drying droplet in supercritical carbon dioxide enriched with ethanol.

Keywords: Atomisation; Lysozyme; Particle size distribution; Mass transfer; Computational fluid dynamics

1. Introduction

The necessity for appropriate protein stabilisation methods increases as the number of labile protein based therapeutics being approved and introduced to the market is greater than ever [1]. Proteins are often unstable in liquid formulations because of chemical and physical degradation reactions [1], and traditional drying processes such as freeze- or spray-drying potentially cause harmful stresses on them [2]. The use of supercritical fluid (SCF) as drying medium for the precipitation of proteins had been previously suggested because of the mild process conditions [3].

Despite the poor solubility of water in supercritical carbon dioxide (SC-CO_2), the production of protein powders from aqueous solution is favoured over drying from organic solutions as organic solvents can negatively affect protein stability [4] and are often poor at dissolving proteins. Drying of aqueous protein solutions by SCF has been reported by several authors [5]. The influence of process flow rates on the particle morphology was recently demonstrated using lysozyme as solute [6]. In that study, three

* Corresponding author. Process Equipment, Delft University of Technology, Leeghwaterstraat 44, 2628 CA Delft, The Netherlands. Tel.: +31 15 278 5561; fax: +31 15 278 6975.
E-mail address: a.m.j.l.bouchard@tudelft.nl (A. Bouchard).

0939-6411/$ - see front matter © 2008 Elsevier B.V. All rights reserved.
doi:10.1016/j.ejpb.2008.03.020

regimes of particle formation were identified and the effect of the process conditions on particle morphology was mainly attributed to the anti-solvent effect of the ethanol added to the CO_2 to increase the water solubility, and to the water evaporation from the droplet. In previous studies various types of nozzles – such as T-mixers [7,8], coaxial nozzles [8–11] and ultrasonic nozzles [12,13] – were used. Yet, no systematic comparison of their impact on the particulate product has been presented except for a slight effect on the particle size [8,13]. In the study presented here, lysozyme was selected as a model compound as it can be produced as amorphous particles in various, generally spherical, morphologies simply by changing the ratio of the flow rates [6].

The particle size has been investigated by other researchers in some systems where the solute was dissolved in an organic solvent and then sprayed into SC-CO_2 for precipitation. However, many parameters were often modified simultaneously making the interpretation of the results difficult. It seemed that the increase in concentration of the solute caused an increase in particle size [9]. The combined increase in pressure and decrease in SC-CO_2 flow rate also caused an increase in particle size. In a more complete study with polymers, Mawson et al. observed that the particles produced with a coaxial nozzle were larger than when a simple capillary was used. They also observed an increase in particle size when increasing the solute concentration whereas using a poorer solvent appeared to cause a reduction of the particle size. Reverchon and Della Porta observed the same decreasing effect of the solvent and the solute concentrations on particle diameter with pharmaceutical compounds in a system where the solution was atomised through a capillary [14]. In a comparative study where yttrium acetate was precipitated from DMSO using SC-CO_2, it was shown that the particle size slightly increased with the diameter of the nozzle, the solute concentration or the pressure, but slightly decreased with the temperature [15].

A significant difference between organic solvents and water is their miscibility with SC-CO_2. The organic solvents used in the studies just mentioned are totally miscible with the SC-CO_2 in all proportions. Therefore, distinct droplets of the two liquids are not formed and the mixing of the streams can be described by gaseous mixing. At the opposite, water is almost immiscible with SC-CO_2. Therefore, the linear jet break-up theory is applicable [16]. When ethanol is added to SC-CO_2 the solubility of water in the SCF phase increases [17–19] and the system becomes partially to totally miscible, depending on the ethanol fraction. In such a ternary mixture, it can be expected that the atomisation process will be an intermediate between the two extremes of miscibility.

The aim of this work was to gain insight into the effects of the nozzle type and the fluid flow rates on the atomisation step of the SCF-drying process. We tried to establish whether computational fluid dynamics (CFD) can be used to evaluate the effect of the nozzle on a spray of ethanol in CO_2 and to determine if it can be an appropriate tool to predict the size of SCF-dried particles. We indirectly investigated the effect of five nozzles, the density of the SCF and the total fluid flow rate at constant ratio on the droplet diameter by measuring the resulting particle size distribution by laser diffraction. We also attempted to correlate the results of the constant ratio to the atomisation capacity of the nozzles and to establish the major parameters influencing the droplet size. Furthermore, we experimentally studied the effect of the individual flow rates on the particle size distribution and explained our results through modelling of the mass transfer during the SCF-drying of a droplet.

2. Materials and methods

2.1. Materials

Lyophilized hen egg white lysozyme (~70,000 U/mg) was purchased from Fluka (Switzerland) and kept as per supplier recommendations until use. Technical grade ethanol (100%, Chemproha, The Netherlands) was used and CO_2 (grade 3.5) was purchased from Hoek Loos (The Netherlands). Aqueous solutions of lysozyme were prepared by dissolving the 2% w/w lysozyme in reverse osmosis water. About 15 g of solution was used in each experiment.

2.2. Preparation of particles by SCF-drying

2.2.1. Experimental set-up

A scheme of the experimental set-up is given in Fig. 1. CO_2 was supplied with a diaphragm pump and ethanol was added with a piston pump (Gilson). Both flows were mixed into a T-mixer before entering the thermostated particle formation vessel through the atomisation device. The flow rate of this mixture was controlled to establish the desired conditions regarding the temperature (310 K) and pressure in the precipitation vessel before the aqueous lysozyme solution was added to the CO_2–ethanol stream at the atomisation device, using a syringe pump (Isco). Five different atomisation devices were tested: coaxial converging nozzle with (C+) (Fig. 2A) or without mixing chamber (C−) (Fig. 2B), or a coaxial converging–diverging nozzle with (Sonimist model HSS-600, Misonix Inc., average droplet diameter 8 μm) (CD+) (Fig. 2D) or without (CD−) (Fig. 2C) ultrasonic wave generator, and T-mixer (T) (Fig. 2E). The dimensions of the atomisation devices are listed in Table 1. Because of the capacity of the CO_2 and ethanol pumps, the SCF flow rate used with the CD+ nozzle in this study was at least 40-times lower than what the nozzle is designed for. Furthermore, the properties of the SCF, especially the density, are different from gas at atmospheric conditions. Hence, we simply considered that the shape of the CD+ nozzle could offer extra mixing capacity over the CD− nozzle.

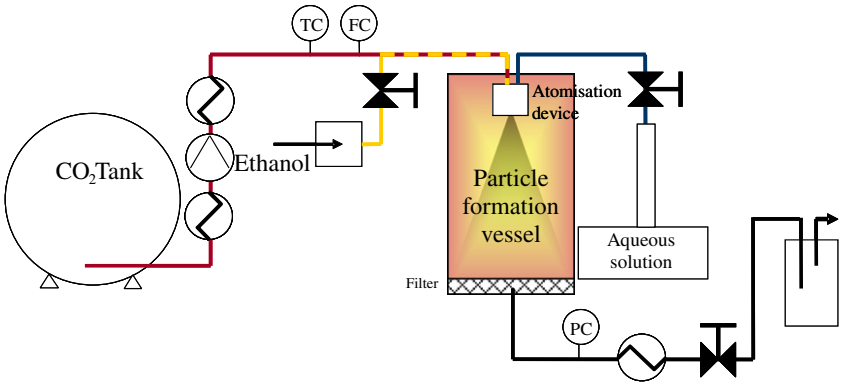

Fig. 1. Basic scheme of the experimental set-up (TC, temperature controller; FC, flow controller and PC, pressure controller). The atomisation devices are illustrated in Fig. 2.

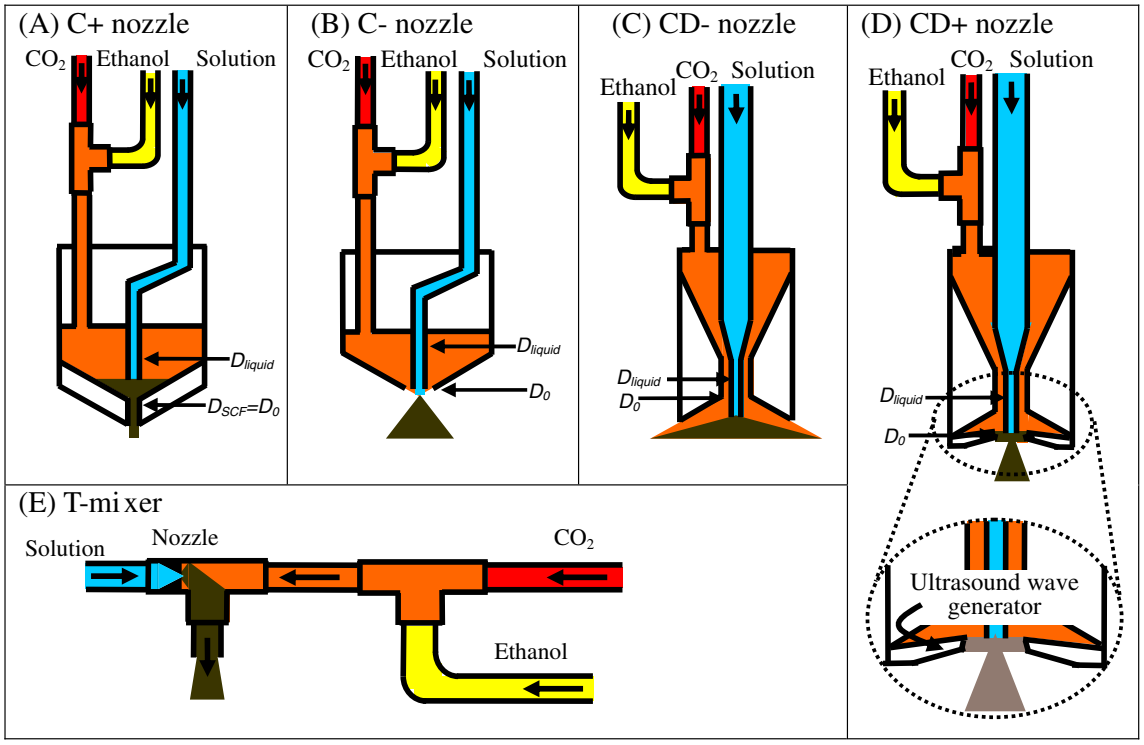

Fig. 2. Schematic presentation of the atomisation devices used in SCF-drying: (A) coaxial converging nozzle with internal mixing chamber (C+), (B) coaxial converging nozzle without internal mixing chamber (C–), (C) coaxial converging–diverging nozzle without ultrasonic wave generator (CD–), (D) coaxial converging–diverging nozzle with ultrasonic wave generator (CD+) and (E) T-mixer (T).

Table 1
Nozzle dimensions as illustrated in Fig. 2

Nozzle	Internal diameter D_{liquid} (mm)	Outer diameter D_{SCF} (mm)	Effective diameter for the SCF phase D_0 (mm)
C–	0.75	1.5	0.75
C+	0.75	1.3	1.3
CD–	0.15	1.1	0.85
CD+	0.15	1.1	0.85
T	0.08	–	–

In the cases of coaxial nozzles (C+, C–, CD+ and CD–), the aqueous solution was injected through the inner tube (indicated as diameter D_{liquid} in Fig. 2) co-currently to the SCF flow injected through the outer section (indicated as diameter D_{SCF} in Fig. 2). The nozzle used in the T-mixer assembly (1/4″) had an opening through which the aqueous solution was injected. The solution was sprayed counter-currently to the SCF mixture through an orifice sapphire nozzle (Fig. 2E). The exit valves were used to control the pressure (10 or 20 MPa) in the 4-L precipitation vessel. After the completion of the spraying process, the vessel was flushed with sufficient CO_2 (at least twice the volume of the vessel) to remove the residual ethanol before depressurisation and product recovery from the filter of the precipitation vessel.

2.2.2. SCF-drying conditions

An array of process conditions was investigated to determine the effect of the process conditions on the morphology of the particles and the particle size distribution (Table 2). The effect of the design of the nozzle was investigated using a standard set of conditions named N1. The operating pressure of SCF-drying was modified to determine the effect of the density (D1 and D2). The ratio between flow rates was kept constant while changing the total flow rate to identify the hydrodynamics effect (H1–H4). The flow rates of the various streams were also independently varied to determine the individual effect of the streams while SCF-drying lysozyme (F1–F4).

2.3. Particle characterisation

2.3.1. Particle size analysis

Geometric particle size distributions were measured using a HELOS BF-MAGIC laser diffraction apparatus with standard Windox software (Sympatec, Clausthal-Zellerfeld, Germany). Roughly, 0.2 g of powder was disposed into the sample ring of the RODOS dry powder disperser (Sympatec). The powder was then projected through the laser beam for diffraction analysis using compressed air at 300 kPa. For the measurements, a 100-mm lens was used and calculations were made with the Fraunhofer theory. With triplicate measurements, a standard deviation of 0.006, 0.01 and 0.04 μm was calculated, respectively, for x_{10}, x_{50} and x_{90}.

2.3.2. Scanning electron microscopy (SEM)

The morphology of the particles was examined using a scanning electron microscope (Jeol JSM-5400). Particles were fixed to the specimen holder with conductive double sided tape before sputtering them with a thin layer of gold.

2.4. Computational

2.4.1. Calculation of dimensionless numbers

Dimensionless numbers were used to evaluate the relative importance of fluid characteristics in a system. The Reynolds number (*Re*) is defined as the ratio of inertial forces to the viscous forces. The Weber number (*We*) describes the relative importance of the inertia of a fluid compared to its surface tension in a system composed of multiple flows separated by an interface, especially for strongly curved surfaces like droplets. The Ohnesorge number (*Oh*) relates the viscous and surface tension forces and is used in combination with the *Re* or the *We* number to map the various regimes of drop formation in the field of spray technology [20]. The *Re*, *We* and *Oh* numbers were calculated for the liquid and the SCF phases for all process conditions. The effective diameter of the SCF stream (D_0) was used for the calculation of the dimensionless numbers of the SCF phase. These numbers are calculated as

$$Re_{\text{liquid}} = \frac{\rho_{\text{liquid}}(v_{\text{liquid}})D_{\text{liquid}}}{\eta_{\text{liquid}}} \tag{1}$$

$$Re_{\text{SCF}} = \frac{\rho_{\text{SCF}}(v_{\text{SCF}} - v_{\text{liquid}})D_0}{\eta_{\text{SCF}}} \tag{2}$$

$$We_{\text{liquid}} = \frac{\rho_{\text{liquid}}(v_{\text{liquid}})^2 D_{\text{liquid}}}{\sigma} \tag{3}$$

$$We_{\text{SCF}} = \frac{\rho_{\text{SCF}}(v_{\text{SCF}} - v_{\text{liquid}})^2 D_0}{\sigma} \tag{4}$$

$$D_0 = \sqrt{D_{\text{SCF}}^2 - D_{\text{liquid}}^2} \tag{5}$$

$$Oh = We/Re = \frac{\eta_{\text{liquid}}}{\sqrt{\sigma \rho_{\text{liquid}} D_{\text{liquid}}}} \tag{6}$$

Table 2
List of process conditions used in experimental and modelling studies

Conditions	CO_2		Ethanol		Solution		Pressure
	kg/s	m^3/s	kg/s	m^3/s	kg/s	m^3/s	MPa
Nozzle comparison							
N1	6.1×10^{-3}	8.9×10^{-6}	3.3×10^{-4}	4.2×10^{-7}	1.7×10^{-5}	1.7×10^{-8}	10
Density							
D1 (N1)	6.1×10^{-3}	8.9×10^{-6}	3.3×10^{-4}	4.2×10^{-7}	1.7×10^{-5}	1.7×10^{-8}	10
D2	7.6×10^{-3}	8.9×10^{-6}	4.1×10^{-4}	2.7×10^{-7}	1.1×10^{-5}	1.1×10^{-8}	20
Hydrodynamics							
H1	8.3×10^{-3}	1.2×10^{-5}	4.5×10^{-4}	5.7×10^{-7}	2.3×10^{-5}	2.3×10^{-8}	10
H2 (N1)	6.1×10^{-3}	8.9×10^{-6}	3.3×10^{-4}	4.2×10^{-7}	1.7×10^{-5}	1.7×10^{-8}	10
H3	3.9×10^{-3}	5.7×10^{-6}	2.1×10^{-4}	2.7×10^{-7}	1.1×10^{-5}	1.1×10^{-8}	10
H4	1.7×10^{-3}	2.4×10^{-6}	9.0×10^{-5}	1.1×10^{-7}	4.5×10^{-6}	4.5×10^{-9}	10
Flow rate - experimental and mass transfer modelling							
F1 (N1)	6.1×10^{-3}	8.9×10^{-6}	3.3×10^{-4}	4.2×10^{-7}	1.7×10^{-5}	1.7×10^{-8}	10
F2	6.1×10^{-3}	8.9×10^{-6}	3.3×10^{-4}	4.2×10^{-7}	2.5×10^{-5}	2.5×10^{-8}	10
F3	6.1×10^{-3}	8.9×10^{-6}	2.6×10^{-4}	3.3×10^{-7}	1.7×10^{-5}	1.7×10^{-8}	10
F4	4.2×10^{-3}	6.1×10^{-6}	3.3×10^{-4}	4.2×10^{-7}	1.7×10^{-5}	1.7×10^{-8}	10
CFD							
CFD1	8.3×10^{-3}	1.2×10^{-5}	5.5×10^{-4}	1.9×10^{-10}	–	–	10

where ρ is the density, v is the velocity, D is the diameter, η is the viscosity and σ is the surface tension. Because of the low solute concentrations, ρ and η of pure water were taken. For the SCF, the value of ρ was estimated with the perturbed hard sphere chain (PHSC) equation of state [21] and η with the method of Lucas [22].

2.4.2. Computational fluid dynamics

CFD calculations were performed using Fluent™ 6.1 software. For simplification purposes because of interfacial phenomena, the simulations describe the mixing of pure SC-CO_2 as the SCF phase and pure ethanol as the liquid phase, introduced, respectively, through the gas (D_{SCF}) and solution (D_{liquid}) inlets of the various nozzle designs (Fig. 2A–D). The calculations were performed under conditions of complete miscibility between SC-CO_2 and ethanol, as it is adequate to compare the nozzle designs and it limits errors related to the not well known interfacial phenomena. The calculations include (A) the fluid flow using the Navier–Stokes momentum conservation equations with a standard k–ε two-equation turbulence model, with composition-dependent density and molecular viscosity, (B) the species transfer using Fick's law of binary diffusion with constant molecular diffusion coefficients with the assumption that the molecular diffusivities are of very minor importance compared to turbulent diffusivities, (C) the energy, assuming isothermal conditions because there are no external sources of heat. The CFD1 conditions listed in Table 2 describe the operating conditions considered in the simulations. The composition dependence of density was calculated with the PHSC [21]. The results of these calculations were correlated with a polynomial, which was then implemented into a user defined function (UDF), used by Fluent to evaluate the density. The viscosities of pure SC-CO_2 and pure ethanol at 310 K and 10 MPa were obtained from the NIST web database [23]. The viscosity of mixtures of ethanol and CO_2 was calculated using the standard Arrhenius power law for viscosities and implemented into a UDF used by Fluent to evaluate the viscosity of mixtures. The diffusivity of ethanol–SC-CO_2 was estimated with the He–Yu correlation for diffusivities in SC-CO_2 [24]. As explained above, the composition dependence of molecular diffusivity was not considered.

2.4.3. Modelling of the mass transfer

A mass transfer model developed for a stagnant water droplet evaporating by SCF-drying [25] was used to evaluate the influence of the ethanol and CO_2 flow rate ratio on the droplet/particle size. The model takes into consideration the mass transfer of water into the SCF phase, and of the CO_2 and ethanol into the droplet. The phase behaviour of the CO_2–water–ethanol ternary system was modelled with the Peng–Robinson equation of state [26] and the Wong–Sandler mixing rule [27], and the mass and energy transport properties were calculated with suitable empirical correlations [28–30]. For comparison purposes, the diameter of the droplet was assumed to be 20 μm for all process conditions. If the actual initial droplet size was smaller, the composition profiles would have the same shape but will be proportionally compressed in time because of the larger surface area of the droplet [25].

3. Results and discussion

3.1. Break-up regime of jet

To identify the type of spray regime of the process the Ohnesorge chart – *Oh* in function of *Re* – was used. The

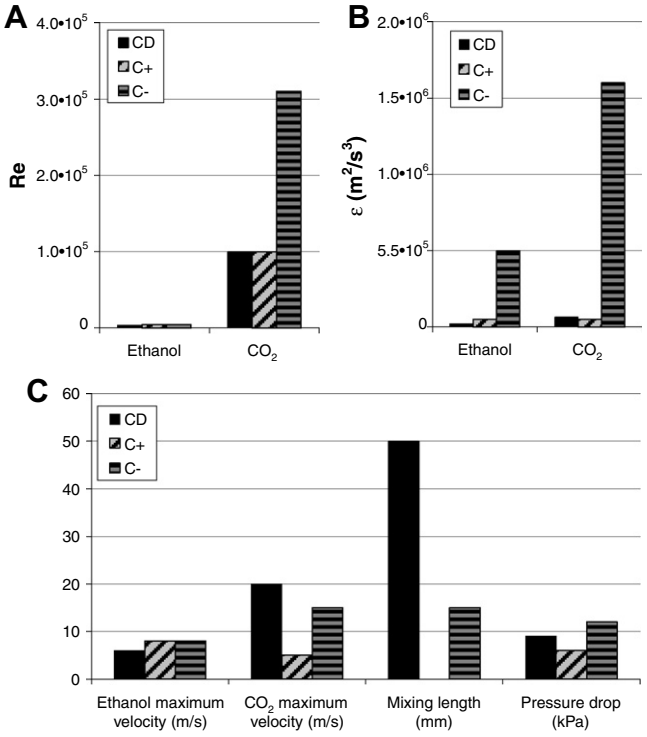

Fig. 3. CFD calculated (A) Reynolds number (*Re*) of ethanol and CO_2, (B) maximum dissipation energy (ε) (m^2/s^3) of ethanol and CO_2, (C) maximum velocity (m/s) of ethanol and CO_2, pressure drop (MPa) across the nozzle, and mixing length (mm) of ethanol and CO_2 at constant flow rate.

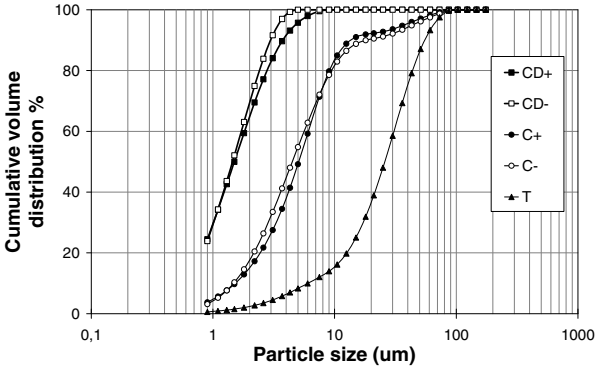

Fig. 4. Cumulative volume distribution (%) curves of lysozyme particles produced at N1 process conditions (see Table 2). CD+, filled square; CD−, empty square; C+, filled circle; C−, empty circle; T, filled triangle.

Oh values calculated for the various nozzles and process conditions were all between 5.15×10^{-3} and 8.53×10^{-3}. According to the Ohnesorge chart [31], all of these conditions should result in the direct atomisation of the solution. This means that the droplets are directly formed at the orifice of the nozzle, and not from the break-up of a jet emerging from the orifice.

3.2. Effect of the nozzle design investigated by CFD

The effect of the design of the nozzles was investigated by CFD based on the *Re* number, the energy dissipation rate and the velocity of the liquid and SCF streams, the pressure drop and the mixing length. The CFD results obtained with the CD− and CD+ were almost identical, and the values reported in Fig. 3 are simply reported as CD. The three designs (C+, C− and CD) gave quite varying results. The highest *Re* number (3×10^5) for the CO_2 was calculated for the C− nozzle (Fig. 3A). From droplet size correlations, the smallest droplets would then be expected from this nozzle [20,32]. This nozzle also led to the highest calculated energy dissipation rate (m^2/s^3) (Fig. 3B). The mixing between the ethanol and CO_2 streams from the outlet of the nozzle (Fig. 3C) was the fastest in the C+ nozzle as it occurred already within the nozzle, followed by the C− nozzle and finally the CD nozzle.

Table 3
Particles characteristic diameters (x_{10}, x_{50} and x_{90} representing 10%, 50% and 90% undersize volume) from various nozzles and process conditions

Nozzle	Conditions	Main effect	x_{10} (μm)	x_{50} (μm)	x_{90} (μm)
Nozzle comparison/density					
CD+	N1/D1	100 bar	0.7	1.5	3.8
CD+	D2	200 bar	0.7	1.4	2.8
CD−	N1/D1	100 bar	0.7	1.5	3.0
CD−	D2	200 bar	0.7	1.4	2.8
C+	N1/D1	100 bar	1.5	5.1	13.8
C+	D2	200 bar	1.7	4.8	12.3
C−	N1/D1	100 bar	1.5	4.5	18.3
C−	D2	200 bar	1.4	3.5	8.7
T	N1	100 bar	6.0	25.9	55.7
Hydrodynamics – total flow rate effect with constant ratio between flow rates					
CD+	H1	8.8×10^{-3} kg/s	0.6	1.2	2.4
CD+	H2	6.5×10^{-3} kg/s	0.7	1.5	3.8
CD+	H3	4.1×10^{-3} kg/s	1.4	3.7	7.9
CD+	H4	1.8×10^{-3} kg/s	1.0	12.6	78.7
CD−	H1	8.8×10^{-3} kg/s	0.6	1.2	4.0
CD−	H2	6.5×10^{-3} kg/s	0.7	1.5	3.0
CD−	H3	4.1×10^{-3} kg/s	1.2	3.0	6.7
CD−	H4	1.8×10^{-3} kg/s	2.7	11.3	31.1
C+	H1	8.8×10^{-3} kg/s	1.4	3.7	10.0
C+	H2	6.5×10^{-3} kg/s	1.5	5.1	13.8
C+	H3	4.1×10^{-3} kg/s	3.0	12.4	44.7
C+	H4	1.8×10^{-3} kg/s	3.9	28.6	84.6
C−	H1	8.8×10^{-3} kg/s	0.9	2.3	5.1
C−	H2	6.5×10^{-3} kg/s	1.5	4.5	18.3
C−	H3	4.1×10^{-3} kg/s	2.2	8.1	35.4
C−	H4	1.8×10^{-3} kg/s	2.5	24.7	74.7
Flow rates – individual flow rate effect					
CD+	F1	Standard	0.7	1.5	3.8
CD+	F2	> Solution	0.7	1.7	4.5
CD+	F3	< Ethanol	0.7	1.9	4.8
CD+	F4	< CO_2	0.8	2.3[a]	6.9
CD−	F1	Standard	0.7	1.5	3.0
CD−	F2	> Solution	0.7	1.7	4.3
CD−	F3	< Ethanol	0.7	1.8	4.4
CD−	F4	< CO_2	1.2	3.0[a]	9.8
C+	F1	Standard	1.5	5.1	13.8
C+	F2	> Solution	1.9	8.6	102.5
C+	F3	< Ethanol	2.3	14.9	75.6
C+	F4	< CO_2	1.7	6.1[a]	42.5
C−	F1	Standard	1.5	4.5	18.3
C−	F2	> Solution	1.5	6.4	63.3
C−	F3	< Ethanol	1.1	4.3	54.8
C−	F4	< CO_2	1.9	5.2[a]	15.8

[a] These particles were not spherical but deformed microparticles.

The atomisation process seems better with the C− nozzle when considering the energy dissipation rate (Fig. 3B), even though the maximum velocity of CO_2 – the drying medium – is the highest in the CD nozzle (Fig. 3C).

The *Re* numbers for the CO_2 stream simply calculated with Eq. (1) (C− ~214,000, C+ ~123,000 and CD ~188,000) were compared to the *Re* numbers calculated by CFD. The *Re* numbers were different, but of the same order of magnitude.

3.3. Effect of the nozzle design investigated experimentally

The five nozzles studied were able to produce microspheres in three different size ranges (Fig. 4). The smallest particles ($x_{50} \sim 1.5$ μm) were obtained with the CD nozzle, and the difference between CD+ and CD− was very small (Table 3 and Fig. 4), indicating that the minor difference in design did not significantly affect the product. Likewise, medium sized particles ($x_{50} \sim 5$ μm) were prepared with either the C+ or the C− nozzles. The T-mixer led to the production of the largest particles ($x_{50} \sim 26$ μm). For all nozzles, complete atomisation of the liquid stream was strongly suggested by the production of individual particles.

If correlating the particle size to the design of the nozzle, the size of the liquid inlet (D_{liquid}) seems of major importance in two-fluid nozzles as particles produced with CD+ and CD− nozzles were much smaller than the particles produced with the C+ and C− nozzles, irrespective of the gas inlet diameter (D_0).

The designs of the CD+, C+ and T nozzles are such that they are prone to accumulation of dry residues because of various edges. This could even result in the complete clogging of the nozzle, especially when processing solutions that produce needle-shaped crystals (e.g., mannitol or glycine). Furthermore, the purpose of the mixing implements of the C+ and CD+ nozzles compared to the C− and CD− nozzles is to reduce the particle size and the width of the distribution. However, none of these implements showed the expected improvement of the particle size and particle size distribution. The lower velocity of the SCF compared to the designed gas velocity (at least 40-times reduction) could be a reason for the insignificant difference in performance between the C+ and CD+ nozzles and the respective C− and CD− nozzles.

The exponential dependence of 0.75 (considering the C and CD nozzles together) of the droplet size on the nozzle dimensions (not shown) is obtained in comparison to 0.40 to 0.55 predicted by droplet size correlations for twin-fluid nozzles [32]. This larger difference observed might be caused due to the difference in design.

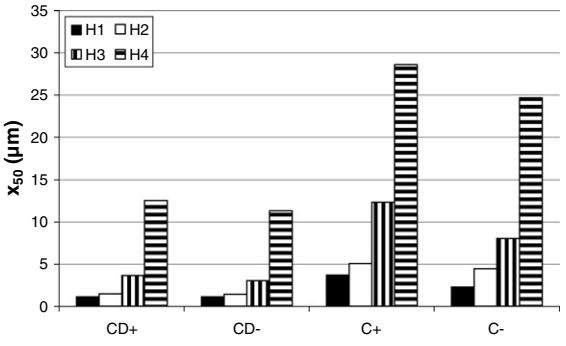

Fig. 5. Median particle geometric diameter, x_{50}, of lysozyme microspheres produced with various nozzles at different total flow rates (H) but constant flow rate ratios. The total ratio in flow rates is such that H1 $(8.8 \times 10^{-3}$ kg/s)/H4 $(1.8 \times 10^{-3}$ kg/s) = 5; H2 $(6.5 \times 10^{-3}$ kg/s)/H4 = 3.7 and H3 $(4.1 \times 10^{-3}$ kg/s)/H4 = 2.3 (see Table 2 for conditions).

3.4. Effect of the total flow rate investigated experimentally

The effect of the hydrodynamics was investigated by producing microspheres with different nozzles and varying the total flow rate while keeping constant the proportionality between the CO_2, ethanol and water flow rates. Increasing the velocity of solution and SCF in the nozzle by increasing the flow rates resulted in the production of smaller particles (Fig. 5), and a narrower particle size distribution (Table 3). An 11- to 12-fold increase in x_{50} was observed with all nozzles when decreasing the flow rates from the maximum (H1: 8.3 g/s CO_2, 0.45 g/s ethanol, 0.023 g/s solution) to the minimum (H4: 1.7 g/s CO_2, 0.09 g/s ethanol, 0.0045 g/s solution), except with C+ for which the increase in x_{50} was only sevenfold.

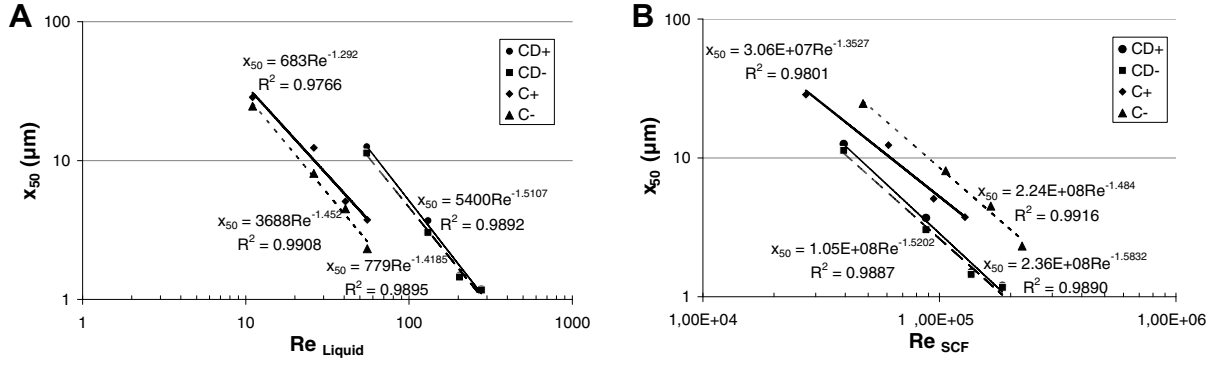

Fig. 6. Median particle geometric diameter (x_{50}) versus the Reynolds number (*Re*) of (A) liquid and (B) SCF phases for constant ratio of flow rates for the CD, C+ and C− nozzles. CD+, circle; CD−, square: C+, diamond; C−, triangle.

The volume density distribution curves of particles produced with the C+ and C− nozzles are bimodal or heavily skewed unimodal, but are normal unimodal for CD+ and CD−. The C+ nozzle shows a significant jump in particle size between the H2 and H3 hydrodynamic conditions (Table 3).

Larger particles and a wider particle size distribution were observed with both the C+ and CD+ nozzles than with the respective C− and CD− nozzles (Table 3). These observations are at the opposite of the intended effect of the mixing chamber: completion of the mixing within the chamber of the C+ nozzle should have the advantage that the mixing is independent of the flow rates.

Re and *We* numbers for both the liquid and the SCF phases were calculated for the various experimental proportional flow rates. The direct relation between the process hydrodynamics and the particle size (x_{50}) for all the nozzles (C+, C−, CD+ and CD−) could be expressed by a power regression (Fig. 6).

The ratio between the flow rates is constant for the results depicted in Fig. 6. Therefore, Fig. 6A shows that the influence of the velocity (v_{liquid}) and nozzle dimensions (D_{liquid}) is important if comparing C and CD nozzles as different ranges of *Re* are covered. However, looking at the slope of the curves which are quite parallel, a similar relative effect of the C and CD nozzles is observed. Even though smaller particles were produced with the CD nozzles, these nozzles can be considered as less efficient than the C nozzles as a higher *Re* number (for the liquid) was calculated for CD than for C nozzles. This is illustrated by the CD curves lying on the right-hand side of the C curves.

The specific effect of various parameters is less distinct in Fig. 6B. The slopes of the curves are quite parallel to each other meaning that the effect of each nozzle is similar. There is a significant overlap of the range of *Re* number such that the velocity (v_{SCF}) and nozzle dimensions (D_0) were of lesser importance than the liquid flow properties. Smaller particles were produced with the CD than with the other nozzles while in the same *Re* range. This can be interpreted as the CD nozzles to be more efficient than the C nozzles. If considering the overall energy requirement of the liquid and SCF streams, the CD nozzles required significantly smaller input of energy than the C nozzles to produce smaller particles.

The difference in the Re_{Liquid} (Fig. 6A) between the CD and C nozzles is more important than the difference in Re_{SCF} (Fig. 6B). Therefore, we can suspect that the liquid stream has a slightly more important effect on the droplet size than the SCF stream, at least with the nozzles investigated. If plotting the particle size versus the relative velocity ($v_{SCF} - v_{liquid}$) (not shown) an exponential dependence of −1.4 to −1.5 is obtained in comparison to −0.9 to −1.2 predicted by droplet size correlations for twin-fluid nozzles [32]. This difference is probably related to the effect of the density of the SCF, compared to the more or less atmospheric gas phase, which is not considered in these correlations.

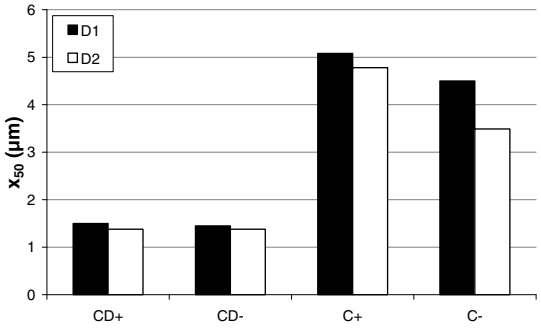

Fig. 7. Median particle geometric diameter, x_{50}, of lysozyme microspheres produced with various nozzles at D1 (10 MPa) and D2 (20 MPa) and equivalent volumetric flow rate (see Table 2 for conditions).

3.5. Effect of the process pressure investigated experimentally

Increasing the working pressure, from 10 MPa ($\rho_{SCF} = 774$ kg/m^3) to 20 MPa ($\rho_{SCF} = 882$ kg/m^3), resulted in a minor to moderate decrease in the median particle diameters. A larger decrease in particle size (∼20%) was obtained with the C nozzles than with the CD nozzles (∼5–8%) (Fig. 7 and Table 3). The overall shape of the % cumulative volume distribution and volume density curves remained similar (not shown), meaning that the particle size distribution of powders obtained with the CD nozzles were unimodal, and that of powders produced with the C nozzle were bimodal.

The decrease in particle size at higher fluid density was expected as the density of the expeller drying fluid should cause a reduction of the droplet size [33]. C Nozzles lead to bimodal particle size distribution with a median small particle peak at 4–7 μm and a median large particle peak at ∼50 μm at 10 MPa or 30–40 μm at 20 MPa (not shown). The decrease in the particle size observed with the C nozzles might be caused by a reduction of the coalescence of the droplet or the reduction in agglomeration of the particles. The density of the drying medium might have improved the dispersion because of its higher resistance towards the liquid stream. The higher pressure of the SCF could also have limited coalescence and agglomeration by favouring a faster drying of the droplet. The higher fluid density might also have assisted the break-up of large droplets.

The exponential dependence of −0.4 to −0.5 (−2 for the C− nozzle) of the droplet size on the gas density (not shown) is obtained in comparison to −0.45 to −0.7 predicted by droplet size correlations for twin-fluid nozzles [32]. In correlations considering the density of the gas phase the hydrodynamics is often ignored [20].

3.6. Independent effect of the process streams investigated experimentally

In addition, experiments were done with various flow rate ratios. The particles obtained with the C+ and C− nozzles at the F2 and F3 conditions showed multimodal

distributions (not shown) and the x_{50} value should not be compared to the other values. Decreasing the CO_2 flow rate (decrease of 30% from F1 to F4) caused the most important increase (30–70%) in particle size (Fig. 8). Increasing the solution flow rate (increase of 50% from F1 to F2) caused a slight increase of the particle size (Fig. 8). Decreasing the ethanol flow rate (decrease of 20% from F1 to F3) resulted in a higher increase of the particle size than what was observed with the solution flow rate (Fig. 8). These results are discussed together with the mass transfer modelling results.

In addition to the particle size distribution, it was observed that the particle shape can change with the ratio between flow rates because of the particle formation mechanism [6]. Microspheres – smooth spherical particles with a dense core – were produced with F1 (Fig. 9A), F2 (Fig. 9B) and F3 (Fig. 9C) conditions, and shrivelled microparticles – micron-scale spheroid, deformed particles or collapsed sphere with a dense shell and porous core – were produced with F4 (Fig. 9D) conditions, independently of the nozzle.

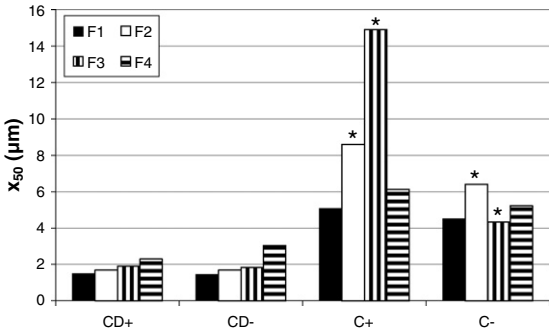

Fig. 8. Median particle geometric diameter, x_{50}, of lysozyme particles produced with various nozzles at various flow rate ratios. *Multimodal particle size distributions. F1, standard conditions; F2, increased solution flow rate by 50%; F3, decreased ethanol flow rate by 20%; F4, decreased CO_2 flow rate by 30% (see Table 2 for conditions).

The plotting of the median diameter (x_{50}) of particles produced with various ratios of process flow rates versus *Re* and *We* of liquid and SCF phases (i.e., Fig. 6) did no show clear trends. The variation in the composition of the fluid had such a strong effect on the particle size that the change in hydrodynamics caused by the variation of one stream was supplanted. However, the independent variation of the stream might not simply affect the particle size distribution because of its effect on the atomisation process, but also the particle formation mechanism.

Considering the effect of the various flow rates on the atomisation process, the following general observations can be made: Reducing the CO_2 flow rate reduces the energy involved in the spraying process and larger droplets would be expected. However, by decreasing the CO_2 flow rate, the ethanol concentration in the SCF is automatically increased, causing a drop in surface tension (from about 10 to 6 mN/m, unpublished results) which should result in the formation of smaller droplets. Therefore, the slight increase in particle size when decreasing the ethanol fraction might be related to the increase in interfacial tension. Increasing the solution flow rate might increase the agglomeration of droplets before or during particle formation. To gain a better understanding of the effect of the various flow rates,

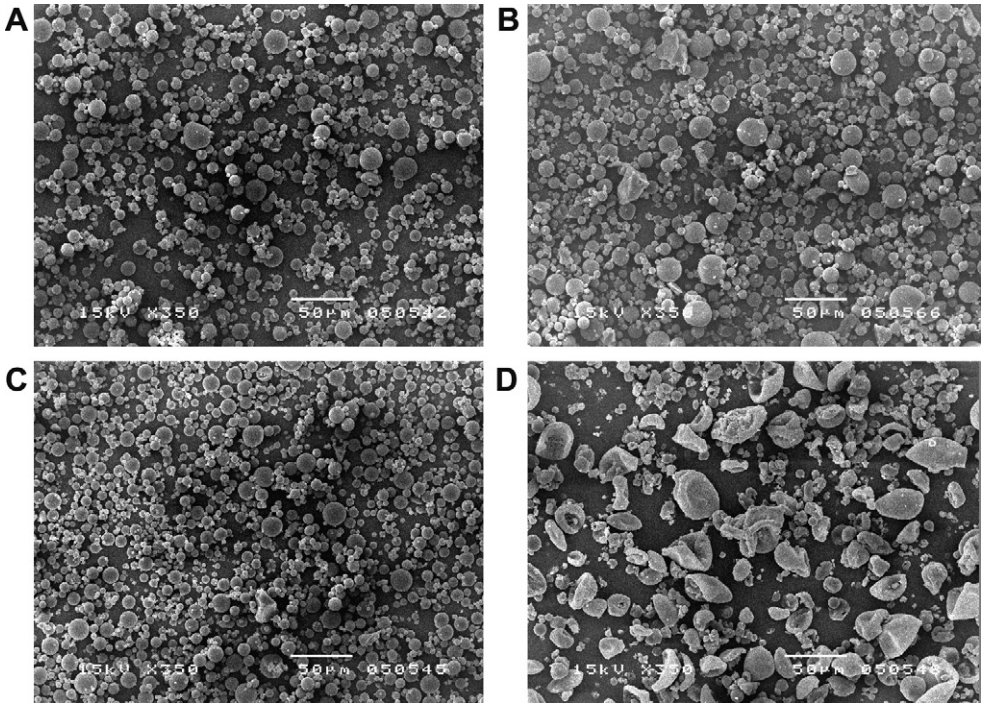

Fig. 9. SEM pictures of microparticles and microspheres produced with CD− nozzle at different flow rate conditions. (A) F1, standard conditions; (B) F2, increased solution flow rate by 50%; (C) F3, decreased ethanol flow rate by 20%; (D) F4, decreased CO_2 flow rate by 30% (see Table 2 for conditions).

the mass transfer around a droplet was investigated by modelling.

3.7. Independent effect of the process streams investigated by modelling

Changing the ratio between the CO_2–ethanol–water flow rates affects the mass transfer in and out of the droplets. The effect can be such that the morphology of the particles can be significantly affected, ranging from smooth microspheres to shrivelled microparticles and ultimately to agglomerates of nanoparticles [6]. Using a simple mass transfer model of a water droplet evaporating in a SCF CO_2–ethanol mixture, the size (Fig. 10) and composition (Fig. 11) of the droplet over time were investigated, and compared to the experimental trend observed for the particle size. The modelling results (Figs. 10 and 11) showed that when some ethanol is added to the SCF phase, the droplet first swells because of condensation and diffusion of ethanol into it, triggering a sharp increase in diffusion of CO_2 into the liquid phase, until the drop starts shrinking as the loss of volume by evaporation becomes greater than the gain. The extent of the swelling stage is proportional to the fraction of ethanol in the extractant (Fig. 10). Assuming the same initial droplet size for all cases, a droplet produced with the F3 and F4 conditions could, respectively, swell 5% and 20% more than a droplet produced with the F1 conditions, which already swells by 12%. The time to complete the evaporation is inversely proportional to the ethanol fraction, and thus inversely proportional to the swelling.

The hydrodynamics effect on the droplet size was indirectly studied by measuring the particle size for constant ethanol:CO_2:solution flow rate ratio. The hydrodynamics will also be affected by independently changing the flow rates (ethanol, CO_2, solution). However, the particle size is probably not simply affected by the droplet size.

First of all, for a constant solution flow, the solubility of water in the SCF phase is decreased when the CO_2 flow is increased as the ethanol:CO_2 ratio is decreased. Since the water uptake capacity of the fluid is sufficient, a lower solubility of water in the SCF shall result into a longer drying time caused by a smaller driving force for evaporation. Finally, the increased number of droplets in the drying medium might favour coalescence of the droplets or agglomeration of the particles.

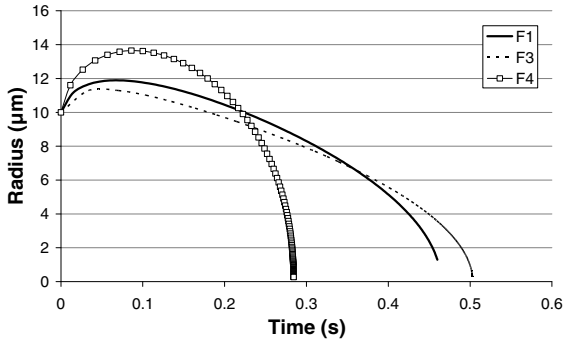

Fig. 10. Modelled water droplet radius during SCF-drying using various ethanol–CO_2 ratios. F1, standard conditions; F3, decreased ethanol flow rate by 20%; F4, decreased CO_2 flow rate by 30% (see Table 2 for conditions).

Secondly, increasing the CO_2 flow rate causes a significant increase in mixing energy. The formation of smaller droplets will then be favoured by the more efficient atomisation. Furthermore, a faster precipitation and lesser coalescence of the droplets are expected because of the rapid attainment of the precipitation conditions.

Thirdly, higher flow rates of CO_2 are associated to higher refreshment rates of the SCF phase. This inherently leads to a higher water uptake capacity which should limit the cohesion of droplets and help maintaining appropriate precipitation conditions in the surroundings of the droplet. However, the higher velocity caused by the higher flow rates also results in a shorter residence time of the SCF phase through the vessel. The flight time for the drops to reach the filter is shortened and there is consequently less time for the particle to be formed before reaching the filter plate. Overall, the increase of energy input in the system when using higher CO_2 and ethanol flow rates was such that a better atomisation was possible, resulting in smaller drops and demonstrated by smaller particles.

The mass transfer modelling was already used to explain the particle formation process of lysozyme particles [6] and the selective precipitation of glycine polymorphs [34,35]. While studying the particle formation process of lysozyme, a main concern that aroused from the particle morphology was the role of the atomisation on the particle formation process (e.g., role of droplet size on the morphology). The composition of the droplet during precipitation was identified as being of major importance for the morphology [6,25] and is therefore suspected to also influence the particle size because of the swelling and shrinking stages of a droplets evaporating in SCF-drying.

The F1 conditions led to the production of the smallest particles irrespective of the nozzle used. When changing the conditions to F3 (lower ethanol ratio), effects on the spray process are expected to be limited to the slight increase in interfacial tension at the water–SCF phase interface and the slight decrease in density of the SCF phase: Between F1 and F3, the decrease in volumetric flow rate of the SCF is only 1%. The very slim changes in density and surface tension were, however, apparently sufficient to cause an increase in particle size in most cases.

Working with F4 (lower CO_2 ratio) conditions, the particle size can increase because of the lower intensity of the atomisation process as the volumetric flow rate of the SCF phase is lower. However, similar results were obtained when the flow rates were doubled. Therefore, the high ethanol fraction in the system is a main factor in the swelling of the droplets. We can suspect that the solidification of the droplet occurred late in the swelling stage or early in the shrinking stage of the droplet drying while the difference in droplet size is the largest (Fig. 10). The high ethanol

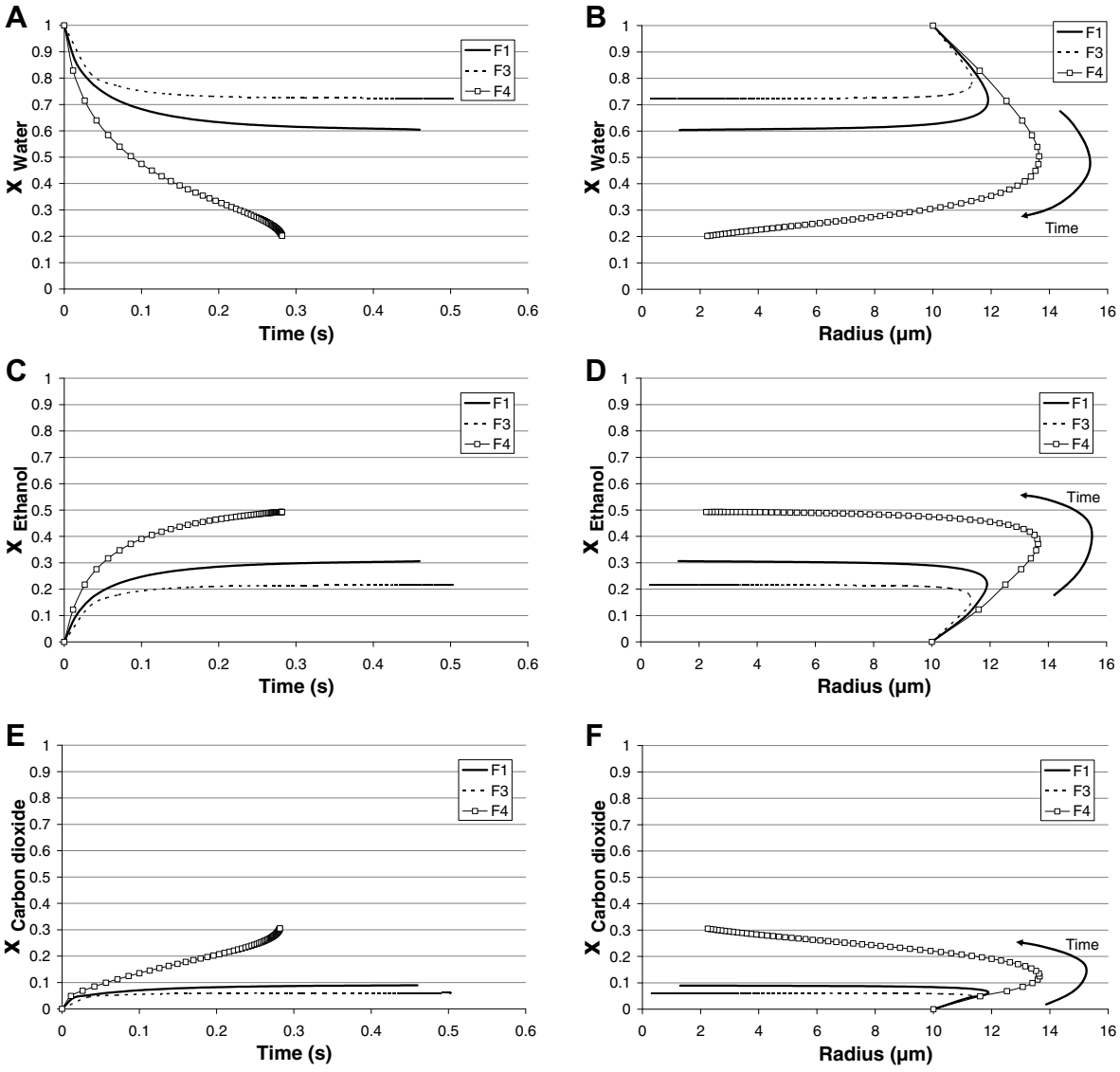

Fig. 11. Modelled composition of water droplets during SCF-drying using various ethanol–CO_2 ratios. F1, standard conditions; F3, decreased ethanol flow rate by 20%; F4, decreased CO_2 flow rate by 30% (see Table 2 for conditions).

fraction in the droplet (F4) also promotes the anti-solvent precipitation of the lysozyme into shrivelled microparticles instead of microspheres.

When changing the initial droplet size, the calculations show that the composition and droplet size remained similar, but occurred on a different time-scale. Therefore, the smaller droplets/particles produced by the CD nozzles might be less prone to coalescence/agglomeration than the larger droplets/particles produced by the C nozzles. Consequently, the increased number of particles of large size (Fig. 8) observed with the C+ and C− nozzles at the F2 conditions is believed to be caused by the coalescence as there is a higher density of droplets in suspension when increasing the solution flow rate. At the F3 conditions, the lower ethanol fraction prolongs the time required for the drying of the droplet and can facilitate the agglomeration of particles.

4. Conclusion

The atomisation step of the SCF-drying behaves more similarly to the atomisation of a liquid into a gas than the gaseous mixing of two streams. The particle size distribution of particles prepared by SCF-drying has shown to be sensitive to the nozzle selection and hydrodynamics. Strongly related to their design and dimensions, the nozzles investigated in this study produced particles with median geometric diameters of ~1.5, ~5 or ~25 μm when using typical SCF-drying conditions. A fivefold increase in the total flow rates (constant ratio between flows of CO_2, ethanol and solution) caused a 7- to 10-fold decrease in particle size. Moreover, the velocity of the liquid stream had a greater effect on the particle size than the velocity of the SCF. The increase in process pressure causes an increase in density of the SCF, and this resulted into a 5–20%

decrease in median particle size because of the higher resistance of expeller fluid. The independent variation in process flow rates also slightly affected the particle size distribution, but to a lesser extent than the hydrodynamics or the nozzle. The time within which the precipitation conditions are reached in the droplet compared to the swelling and shrinking stages occurring during the drying of the droplet could be responsible for the variation in the particle size when the flow rates are modified independently. The similar transition observed with lysozyme from the formation of microspheres to microparticles occurring with all nozzles demonstrates that the particle morphology resulted primarily from the precipitation mechanism of the solute and not from the atomisation process. This control over the median particle size, the particle size distribution and the particle morphology makes the SCF-drying technique a good process to prepare micron-size particles with stringent specifications in respect of size, morphology, density, etc. Both the atomisation device and the process conditions should be selected to fine-tune the desired characteristics of the powder.

In this study the effect of the nozzle and the process conditions on the droplet size was indirectly investigated by measuring the particle size distribution off-line. The three-wavelength-extinction technique investigated by Marioth et al. [36] to measure particle and droplet sizes in SC-CO_2 is a potential on-line technique that could be used for the droplet size measurements. However, this technique would need to be validated before it could be used to develop a good correlation to predict the droplet size produced during SCF-drying. Further, work will be required to estimate the effect of the droplet size on the particle size as the process conditions, but also the compound being precipitated, are expected to influence the powder characteristics.

Acknowledgments

The authors thank Paul Hagedoorn (Department of Pharmaceutical Technology and Biopharmacy, University of Groningen) and Michel van den Brink (Process & Energy, Delft University of Technology) for their assistance in the characterisation of particles. This research was supported by the Technology Foundation, STW, the Applied Science Division of NWO and the Technology Program of the Dutch Ministry of Economic Affairs.

References

[1] M.C. Manning, K. Patel, R.T. Borchardt, Stability of protein pharmaceuticals, Pharm. Res. 6 (1989) 903–918.
[2] J.F. Carpenter, M.C. Manning, Rational Design of Stable Protein Formulations, Theory and Practice, Kluwer Academic/Plenum Publishers, New York, 2002.
[3] S.D. Yeo, G.B. Lim, P.G. Debenedetti, H. Bernstein, Formation of microparticulate protein powders using a supercritical fluid antisolvent, Biotechnol. Bioeng. 41 (1993) 341–346.
[4] M. Jackson, H.H. Mantsch, Beware of proteins in DMSO, Biochim. Biophys. Acta 1078 (1991) 231–235.
[5] N. Jovanovic, A. Bouchard, G.W. Hofland, G.-J. Witkamp, D.J.A. Crommelin, W. Jiskoot, Stabilization of proteins in dry powder formulations using supercritical fluid technology, Pharm. Res. 21 (2004) 1955–1969.
[6] A. Bouchard, N. Jovanović, W. Jiskoot, E. Mendes, G.-J. Witkamp, D.J.A. Crommelin, G.W. Hofland, Lysozyme particle formation during supercritical fluid drying: particle morphology and molecular integrity, J. Supercrit. Fluids 40 (2007) 293–307.
[7] A. Bouchard, N. Jovanovic, G.W. Hofland, D.J.A. Crommelin, W. Jiskoot, G.-J. Witkamp, Supercritical drying of lysozyme from aqueous solution, in: G. Brunner, I. Kikic, M. Perrut (Eds.), Sixth International Symposium on Supercritical Fluids, Versailles, France, 2003, pp. 1949–1952.
[8] A. Bouchard, N. Jovanovic, G.W. Hofland, D.J.A. Crommelin, W. Jiskoot, G.-J. Witkamp, Nozzle selection and optimisation of process conditions for the supercritical-drying of lysozyme, in: I. Kikic, M. Perrut (Eds.), Ninth Meeting on Supercritical Fluids, Trieste, Italy, June 13–16, 2004, pp. 41.
[9] S. Mawson, S. Kanakia, K.P. Johnston, Coaxial nozzle for control of particle morphology in precipitation with a compressed fluid antisolvent, J. Appl. Polym. Sci. 64 (1997) 2105–2118.
[10] M.H. Hanna, P. York, Methods and apparatus for the formation of particles, US 6440337, 2002.
[11] G. Del Re, M. Putrignano, G. Di Giacomo, C. Di Palma, Apparatus and method for micron and submicron particle formation especially for proteins of pharmaceutical interest, WO 0268107, 2002.
[12] R.B. Gupta, P. Chattopadhyay, Method of forming nanoparticles and microparticles of controllable size using supercritical fluids and ultrasound, US 20020000681, 2002.
[13] R.T. Bustami, H.K. Chan, T. Sweeney, F. Dehghani, N.R. Foster, Generation of fine powders of recombinant human deoxyribonuclease using the aerosol solvent extraction system, Pharm. Res. 20 (2003) 2028–2035.
[14] E. Reverchon, G. Della Porta, Particle design using supercritical fluids, Chem. Eng. Tech. 26 (2003) 840–845.
[15] E. Reverchon, G. Caputo, I. De Marco, Role of phase behavior and atomization in the supercritical antisolvent precipitation, Ind. Eng. Chem. Res. 42 (2003) 6406–6414.
[16] C.S. Lengsfeld, J.P. Delplanque, V.H. Barocas, T.W. Randolph, Mechanism governing microparticle morphology during precipitation by a compressed antisolvent: atomization vs. nucleation and growth, J. Phys. Chem. B 104 (2000) 2725–2735.
[17] S. Yao, Y. Guan, Z. Zhu, Investigation of phase equilibrium for ternary systems containing ethanol, water and carbon dioxide at elevated pressures, Fluid Phase Equilib. 99 (1994) 249–259.
[18] S. Takishima, K. Saiki, K. Arai, S. Saito, Phase equilibria for the carbon dioxide–ethanol–water system, J. Chem. Eng. Jpn. 19 (1986) 48–56.
[19] M.L. Gilbert, M.E. Paulaitis, Gas–liquid equilibrium for ethanol–water–carbon dioxide mixtures at elevated pressures, J. Chem. Eng. Data 31 (1986) 296–298.
[20] H. Liu, Science and Engineering of Droplets: Fundamentals and Applications, Noyes/William Andrew, Park Ridge, 2000.
[21] Y. Song, S.M. Lambert, J.M. Prausnitz, A perturbed hard-sphere-chain equation of state for normal fluids and polymers, Ind. Eng. Chem. Res. 33 (1994) 1047–1057.
[22] B.E. Poling, J.M. Prausnitz, J.P. O'Connell, The Properties of Gases and Liquids, McGraw-Hill Higher Education, Singapore, 2001.
[23] E.W. Lemmon, M.M.O, D.G. Friend, Thermophysical properties of fluid systems, in: P.J. Linstrom, W.G. Mallard (Eds.), NIST Chemistry WebBook, National Institute of Standards and Technology, Gaithersburg, MD, June 2005. Available from: <http://webbook.nist.gov/chemistry/>.
[24] C.-H. He, Y.-S. Yu, New equation for infinite-dilution diffusion coefficients in supercritical and high-temperature liquid solvents, Ind. Eng. Chem. Res. 37 (1998) 3793–3798.

[25] Á. Martín, A. Bouchard, G.W. Hofland, G.-J. Witkamp, M.J. Cocero, Mathematical modeling of the mass transfer from aqueous solutions in a supercritical fluid during particle formation, J. Supercrit. Fluids 41 (2007) 126–137.
[26] D.-Y. Peng, D.B. Robinson, A new two-constant equation of state, Ind. Eng. Chem. Res. 15 (1976) 59–64.
[27] D.S.H. Wong, S.I. Sandler, A theoretically correct mixing rule for cubic equations of state, AIChE J. 38 (1992) 671–680.
[28] C.J. Chang, K.-L. Chiu, C.-Y. Day, A new apparatus for the determination of *P–x–y* diagrams and Henry's constants in high pressure alcohols with critical carbon dioxide, J. Supercrit. Fluids 12 (1998) 223–237.
[29] B. Yang, H. Wang, Vapor–liquid equilibrium for mixtures of water, alcohols, and ethers, J. Chem. Eng. Data 47 (2002) 1324–1329.
[30] A. Bamberger, G. Sieder, G. Maurer, High-pressure (vapor–liquid) equilibrium in binary mixtures of (carbon dioxide + water or acetic acid) at temperatures from 313 to 353 K, J. Supercrit. Fluids 17 (2000) 97–110.
[31] K. Masters, Spray Drying, Hill, London, 1972.
[32] J.R. Fair, D.E. Steinmeyer, W.R. Penney, B.B. Crocker, Gas absorption and gas–liquid system design, in: R.H. Perry, D.W. Green (Eds.), Perry's Chemical Engineer's Handbook, The McGraw-Hill Companies, Inc., New York, 1997.
[33] A.H. Lefebvre, Atomization and Sprays, Hemisphere Publishing Corporation, New York, 1989.
[34] A. Bouchard, N. Jovanović, G.W. Hofland, D.J.A. Crommelin, W. Jiskoot, G.-J. Witkamp, Ways of manipulating the polymorphism of glycine during supercritical fluid crystallization, J. Supercrit. Fluids 44 (2008) 422–432.
[35] A. Bouchard, N. Jovanović, G.W. Hofland, E. Mendes, D.J.A. Crommelin, W. Jiskoot, G.-J. Witkamp, Selective production of polymorphs and pseudomorphs using supercritical fluid crystallization from aqueous solutions, Cryst. Growth Des. 7 (2007) 1432–1440.
[36] E. Marioth, B. Koenig, H. Krause, S. Loebbecke, Fast particle size and droplet size measurements in supercritical CO_2, Ind. Eng. Chem. Res. 39 (2000) 4853–4857.